

An effective control approach of hybrid energy storage system based on moth flame optimization

V. Prasanna, G. Ravi

Department of Electrical and Electronics Engineering, Puducherry Technological University, Puducherry, India

Article Info

Article history:

Received Apr 24, 2023

Revised Jun 21, 2023

Accepted Jun 28, 2023

Keywords:

Energy storage system

Hybrid energy system

Moth flame algorithm

PV-wind system

REPS

Supercapacitor

ABSTRACT

In modern days, renewable sources increase the independence of urban energy infrastructures from remote sources and grids. In renewable energy systems (RES) systems, batteries are frequently used to close the power gap between the power supply and the load demand. Due to the variable behavior of RES and the fluctuating power requirements of the load, batteries frequently experience repeated deep cycles and uneven charging patterns. The battery's lifespan would be shortened by these actions, and increase the replacement cost. This research provides an effective control method for a solar-wind model with a battery-supercapacitor hybrid energy storage system in order to extend battery's lives expectancy by lowering intermittent strain and high current need. Unlike traditional techniques, the suggested control scheme includes a low-pass filter (LPF) and a fuzzy logic controller (FLC). To begin, LPF reduces the fluctuating aspects of battery consumption. FLC lowers the battery's high current need while continuously monitoring the supercapacitor's level of charge. The moth flame optimization (MFO) optimizes the FLC's membership functions to get the best peak current attenuation in batteries. The proposed model is compared to standard control procedures namely rule based controller and filtration-based controller. When compared to the conventional system, the suggested method significantly reduces peak current and high power of the battery. Furthermore, when compared to standard control procedures, the suggested solution boosts supercapacitor utilization appreciably.

This is an open access article under the [CC BY-SA](#) license.



Corresponding Author:

V. Prasanna

Department of Electrical and Electronics Engineering, Puducherry Technological University

Puducherry, India

Email: text2prasanna@gmail.com

1. INTRODUCTION

In renewable energy systems (RES), batteries are frequently used to close the power gap between power supply and load demand. Because of the variable behavior of RES and the inconsistent power need of the load, a battery will typically experience frequent deep cycles and uneven charging patterns. These activities would drain the battery's lifespan and raise the replacement cost [1]–[3]. As a result, the hybrid energy storage is a feasible way for decreasing battery strain, battery capacity, and overall system cost [4]. Specific power, response time specific energy, and durability are all supplementary features of a battery and a supercapacitor (SC). Because it is the program that governs the power of the SC and battery, a management technique is required for the battery-SC model to maximize energy consumption and energy conservation. One of the most typical goals of hybrid energy storage system (HESS) deployment is to increase the lifespan of the battery by lowering peak current needs and constant stress [4], [5]. Reduced peak current in the battery would help lessen voltage drop and enhance battery efficiency. The over-heating and dynamic strain of the

battery are minimized when the stress of the battery is reduced [5], [6]. The use of a fuzzy logic controller (FLC) with a battery-hydrogen storage system (HSS) is popular. Yet, there hasn't been much research about using FLC in RES with battery-SC System. FLC is simple to comprehend and is unaffected by changes in the settings. Furthermore, it does not necessitate a precise system and training process model. Furthermore, when compared to a battery-only system, the FLC minimizes battery capacity loss by more than half [7]. The FLC's membership functions (MFs), on the other hand, are not optimized and do not provide efficient result. The membership functions of FLC are normally evaluated using a time-consuming and inefficient trial-and-error process [8], [9]. Various technologies, like artificial neural networks (ANN) and support vector machines, can be used to estimate solar irradiance and electrical load (SVM) [10]–[15]. As a result, evolutionary algorithms like moth flame optimization (MFO) and others are used in improving the membership functions of the controller in order to address various optimization issues.

The best control model for a PV-wind power system with battery-SC is proposed in this research. The suggested control model's goals are to lower the battery's fluctuating active strain and high current need while keeping the SC's SOC level in mind at all times (SOCsc). A Sugeno-type FLC is used in the proposed control approach. The Sugeno-type FLC is efficient and robust and complements optimization and adaptive approaches well [16]. As a result, it is employed to lower the battery's high current demand by adjusting the the amount of power that the SC will charge/discharge depending on real-time power need and SOCsc. The moth flame algorithm optimization (MFO) is used to find the best FLC MFs in order to decrease high current of the battery. Simulink is utilized to compare the proposed system's performance against that of older systems using a rural household load profile. This paper shows the suggested system's Simulink models and describes the MFO optimization findings as well as the comparison between conventional and proposed systems.

2. SYSTEM MODELLING AND COMPONENTS

A solar panel, a wind turbine, and a battery (lithium ion) are all part of the proposed hybrid system, which also includes a SC. As indicated, all of the elements are coupled to a voltage unified DC bus.

2.1. Wind turbine modelling

In this study, we'll use a wind turbine powered by a permanent synchronous generator (PMSG). The wind turbine's power and rated wind velocity are 300 W and 13 m/s, respectively. The maximum wind velocity is 18 m/s, with a beginning wind velocity of 3 m/s. The maximal power production is 800 W [17].

The output power of a wind turbine can be stated as follows using aerodynamic theory.

$$P = 0.5\rho\pi R^2 V^2 C_{mwp}(\lambda, \beta) \quad (1)$$

Where P_m is the resultant power of a wind turbine generator. The air density, wind speed and blade radius are represented by, R , and V_w , discretely. The power coefficient (C_p), is defined as (2) and (3).

$$C_p(\lambda, \beta) = 0.73 (151/\lambda - 0.58\beta - 0.002\beta^{2.14} - 13.2)e^{-18.4/\lambda} \quad (2)$$

Where:

$$\lambda = 1 / (1/(\lambda - 0.02\beta) - 0.003/(\beta^3 + 1)) \quad (3)$$

In MATLAB, a fluctuating wind of 13 m/s is generated and shown in Figures 1 and 2(a). The wind turbine's output power under MPPT control is displayed [17].

2.2. PV array modelling

A solar array is formed by connecting numerous parallel and series solar cells. To compute the short-circuit current for every solar cell can use as (4) [18].

$$I_{sc} = I_{sc0}(G/G_0)^\alpha \quad (4)$$

Where I_{sc} and I_{sc0} are the short-circuit currents, G and G_0 are standard solar radiation, respectively. The PV cell's open-circuit voltage as (5).

$$V_{oc} = \frac{V_{oc0}}{1 + \beta \ln \left(\frac{G}{G_0} \right)} \left(\frac{T_0}{T} \right)^\alpha \quad (5)$$

Where V_{oc} and V_{oc0} are the open-circuit voltages under average and normal solar energy G and G_0 , respectively, and T is the PV cell temperature. β is a technology-specific coefficient for PV cells that depicts temperature nonlinear effects. Using cells arranged in series (N_s) and cells arranged in parallel (N_p), the highest power from the solar array can be written as [18] as shown in Figure 2(b).

$$P_{max} = N_p \cdot N_s \frac{\frac{V_{oc0}}{nkTq} - \ln\left(\frac{V_{oc}}{nkTq} + 0.72\right)}{1 + V_{oc0}/nkTq} \cdot \left(\frac{1 - R_s}{V_{oc}/I_{sc}}\right) \cdot V_{oc} \cdot I_{sc} \quad (6)$$

Because both the wind turbine and the solar array create power, the collective power produced may be estimated by summing them together. Furthermore, we presume a constant load need of 1 kW. As a result, the power disparity between produced and needed power by load is P as shown in Figures 2(c) and 2(d).

$$\Delta P = P_{WP} + P_{PV} - P_L \quad (7)$$

P_{WP} , P_{PV} , and P_L are the power output of a wind turbine, power of the solar array, and power demand of the load, discretely as shown in Figure 2(e).

2.3. Battery–SC storage system

An SC, a bidirectional DC-DC converter, control circuitry, and a battery bank are all included in the proposed system's HESS, as shown in the simulation of the solar-wind system with battery-SC system. The Simulink library contains the structure and details of the battery, and supercapacitor models. The battery-SC system described in this work, uses the benefits of both high-power density and energy density storage to accomplish the necessary performance. However, combining the battery-SC as a solitary source of power necessitates a sophisticated conditioning circuitry. Because the SC voltage varies greatly because of its low energy density, the proposed model's battery-SC system is built in a partially active architecture, with a bi-directional DC-DC converter located adjacent to the supercapacitor to isolate the supercapacitor from the rest of the system [19].

The power electronic component is made up of a DC-DC converter and control circuits [15]. This design provides enough flexibility to implement a variety of control techniques. Furthermore, with the employment of a single DC-DC converter, this design provides a favorable trade-off between functionality and intricacy of the circuit. It is also necessary to manage the power flow in both directions to properly link the batteries and SCs.

The bidirectional half-bridge DC-DC converter can operate in both buck and boost modes. It comprises of two bi-positional switches constructed in a half bridge arrangement using transistors $S1/S2$ and diodes $D1/D2$. The converter's high and low voltage sides are interfaced to the DC bus and the supercapacitor, to enable for constant functioning of the SC. Power is transmitted from the high to the low voltage side when the converter is in buck mode (inductor current, $i_L > 0$). Power is transmitted from the low to the high voltage side ($i_L < 0$) while the converter is in boost mode as shown in Figure 1. The description of the proposed system's dynamic power balance shown as (8), based on Figure 2.

$$P_{PV} + P_{batt} + P'_{sc} + P_{load} = 0 \quad (8)$$

Where P_{PV} is the PV's power generation, P_{batt} is the battery's power, P_{load} is the load's power demand, and P_{sc0} is the SC power flow after the DC-DC converter's power conversion. The converter's efficiency is less than 100% in real-world operation. As a result, the power shift from the SC to the DC bus written as (9).

$$P'_{sc} = \eta_{DCDC} \times P_{sc} \quad (9)$$

Where P_{sc} denotes SC's power flow and η_{dc} denotes the converter's efficiency. The converter's efficiency is presumed to be 100% in the context of this research. As a result, the amount of power needed by the battery-SC defines as (10), dP , which is the difference between P_{PV} and P_{load} 's output power.

$$dP = P_{PV} - P_{Load} = P_{batt} + P_{sc} \quad (10)$$

Table 1 explains the proposed system parameters. Figure 1 explains the basic structure and Figure 2 shows the profile of the energy management system.

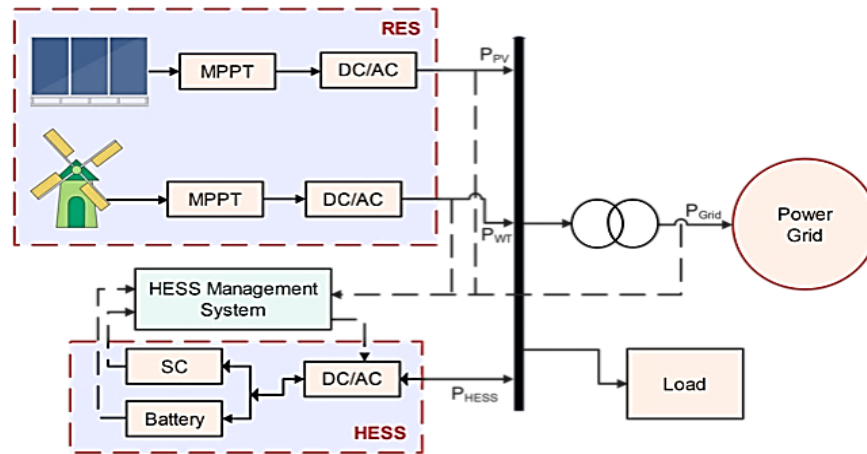


Figure 1. Hybrid energy storage and renewable energy system

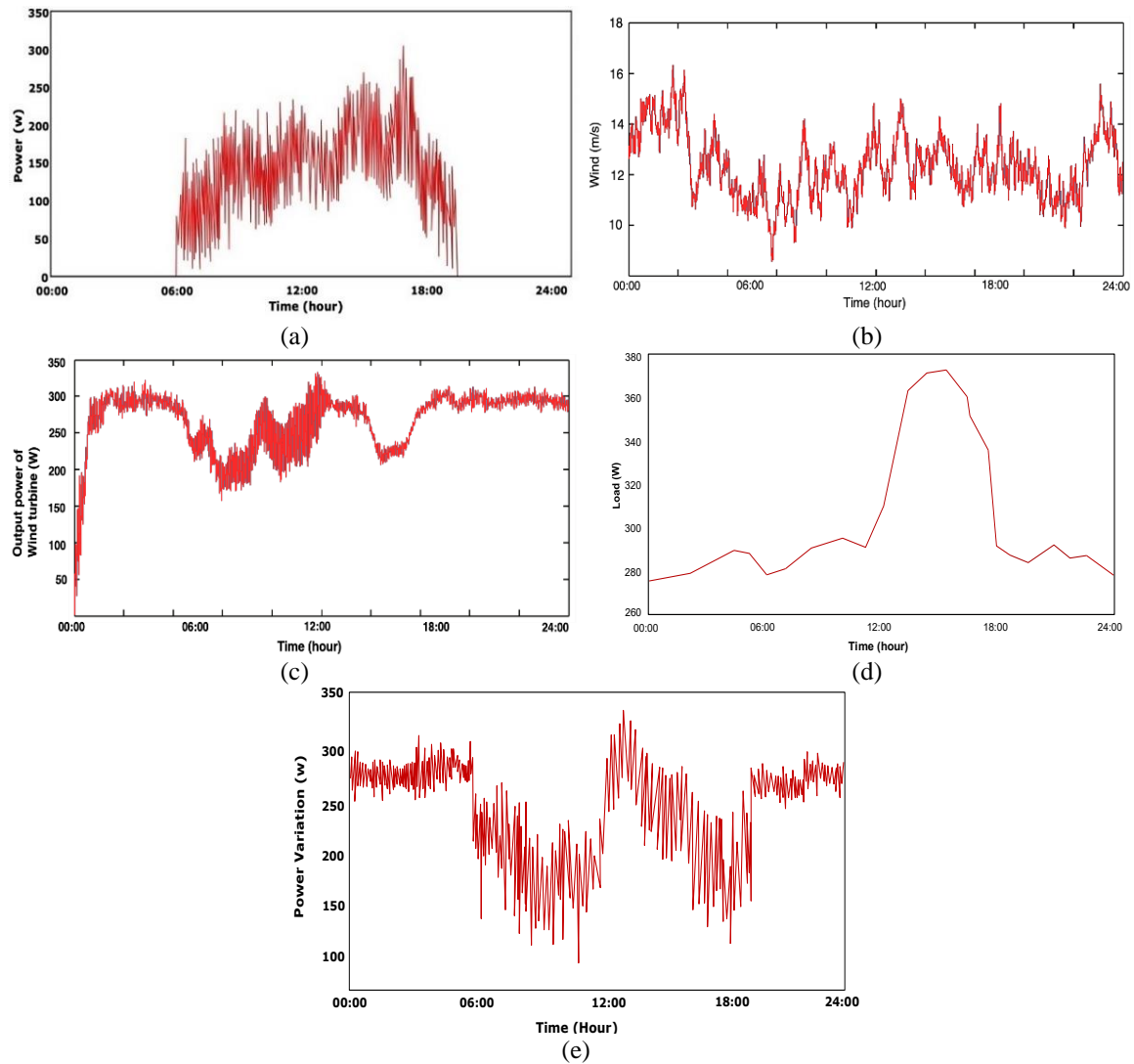


Figure 2. Simulation profiles: (a) solar power output, (b) wind speed, (c) output from wind turbine, (d) load profile, and (e) power variation between power generation and load demand

Table 1. Proposed system's specifications

Component	Rating	Value
PV	Power	1.2kW
Wind system	Power	300 W
Li ion battery	Voltage	48 V
	Capacity	300 Ah
Supercapacitor	Voltage	45 V
	Capacitance	500 F

3. CONTROL STRATEGY

The control strategy, which is based on current system conditions, controls the HESS power flow. In order to accomplish various objectives, it is frequently complicated and calls for constant operation. Optimizing HESS control is essential for maximizing sustainability and energy efficiency [20]–[28]. There are two different categories of control strategies: traditional control techniques and modern control techniques [29]. Rule-based controllers (RBC) and filtering-based controllers (FBC) are examples of traditional control systems that are simple and easy to implement since they don't need intensive processing. But they tend to be rigid and sensitive to parameter changes [30]. Because they develop the dynamic behavior without needing an accurate description of the system, modern control techniques like the FLC are more dependable and effective than traditional control strategies [31]. The MFs of FLC, on the other hand, are normally calculated through trial-and-error, which is ineffective and a lengthy process.

To summarize, renewable energy and energy efficiency portfolio standard (REPS) with battery-supercapacitor HESS frequently use traditional control mechanisms like as RBC and FBC. In this study, the proposed control approach is compared to two common traditional control systems (RBC and FBC). All models with SC have a SOCsc operating range of 50% - 100% to enable for the use of 75% of the total SC energy [32].

3.1. Rule based controller

Based on a set of guidelines, the RBC determines how much power is distributed between the SC and battery. It is easy to implement because it does not necessitate complex processing. RBC, on the other hand, is extremely sensitive to parameter variations due to its pre-defined rules and procedures. An RBC is created and depicted as dead-zone function [33]. Whenever the current of the battery is between the $ib1$ and $ib2$ thresholds, the battery is the sole way to supply the load requirement. when the $ib1$ or $ib2$ threshold is reached for battery current demand, the extra current demand is divided between the SC and the battery according to the $K1$ or $K2$ ratio [33].

3.2. Filtration based controller

The FBC splits the active elements of the power demand into low-frequency and high-frequency parts using a filter. This method is easy and requires little computing power. A high pass filter (HPF)-based FBC's structure [34]. The HPF divides the power requirement into high-frequency (PHF) and low-frequency (PLF) components, with the PHF and PLF fetched by the battery and SC, discretely.

3.3. Proposed control strategy

Figure 3 depicts the framework of the suggested control method, which attempts to reduce the battery's active tension and high current demand. The energy management device in the control strategy is a fuzzy logic controller (FLC). The moth flame optimization (MFO) technique is used to optimize the FLC's membership functions (MFs) in order to obtain optimal performance. The next sections discuss the structure of the suggested control strategy.

3.3.1. DC bus configuration and optimization

The voltage on the DC bus is managed using the principle expressed in Figure 3. The PI device decides the reference current of the DC bus $I_{dc_{ref}}$ to regulate the bus voltage at $V_{ref} = 400$ V. The energy management system (EMS) generates the reference currents for batteries and SCs ($I_{bat_{ref}}$ and $I_{sc_{ref}}$, correspondingly). These reference currents make the DC bus voltage to remain static irrespective of load conduct or fluctuations in power output. When a fault develops on an element such as SoC, power interruption, or solar irradiation variation, the batteries and/or SCs make sure that the DC bus voltage is regulated. The collective reference currents, $I_{sc_{ref}}$ and $I_{bat_{ref}}$, should be same as $I_{dc_{ref}}$ at all times.

$$I_{dc_{ref}} = I_{sc_{ref}} + I_{bat_{ref}} \quad (11)$$

To simulate the function of a DC bus can be used as (12).

$$\frac{C_{dc} dv_{dc}}{dt} = i_{sc_{dc}} + i_{bat_{dc}} - i_{load} \quad (12)$$

The DC currents of SCs, batteries are represented by $i_{sc_{dc}}$, $i_{bat_{dc}}$, respectively. The load current is represented by i_{Load} . C_{dc} is the capacity of the central bus that allows a similar DC bus voltage to be imposed on the load and all other inputs. The power oscillations from the chosen stationary converters are filtered by these capacitors.

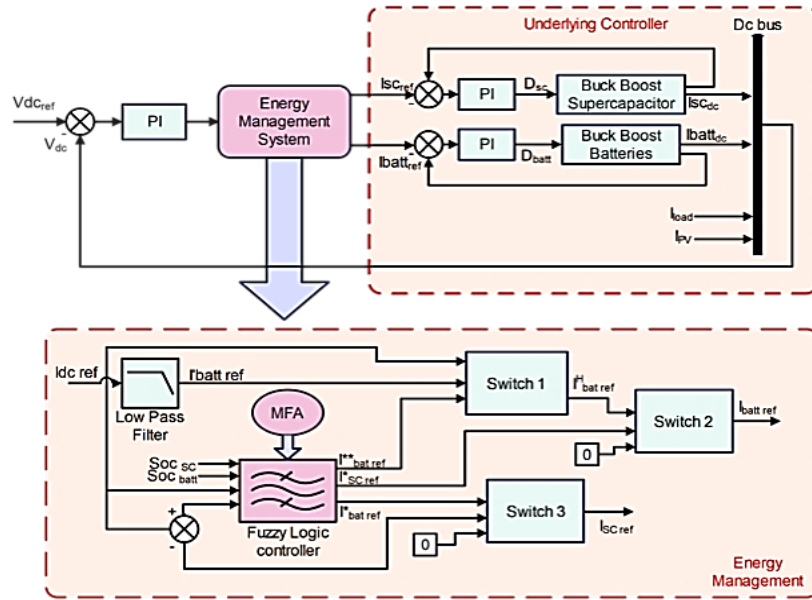


Figure 3. Proposed control strategy

3.3.2. Low pass filter (LPF)

PV power production and load need are very variable in actual operation. To meet the demands of the traditional system's highly fluctuating dP , the battery is put under stress. The extremely variable battery current results in high internal heat of the battery, which would decrease efficiency and increase internal resistance [4]–[6]. LPF is therefore used to break down the dP into P_{HF} and P_{LF} in order to lessen the active load on the battery. The P_{HF} is the mismatch between dP and P_{LF} , while the P_{LF} is the resultant of LPF.

$$P_{LF} = \text{lowpassfilter}(dP) \quad (13)$$

$$P_{HL} = dP - P_{LF} \quad (14)$$

While the SC should ideally handle the P_{HF} , a highly variable power demand, the battery should ideally handle the P_{LF} . This procedure lessens the dynamic stress on the battery by preventing it from delivering the high frequency components. The P_{LF} is sent to the FLC to achieve battery high current attenuation after the LPF filtration.

3.3.3. Fuzzy logic supervisor (FLS)

FLC's goal is to lower battery high current while continuously taking the SOC_{sc} into account. The Sugeno type fuzzy system, which is utilized in this study, is an effective system for computing that functions best with optimization and adaption [16]. The PLF and the SOC_{sc} are the FLC's two inputs, as depicted in Figure 3. The power sharing ratio, which is calculated using the real-time data, is the FLC's output. The inputs' MFs have trapezoidal forms. In Figure 4, the MFs of the FLC are presented.

The five MFs present in the input variable PLF are positive high ("PH"), positive medium ("PM"), low ("L"), negative low ("NL"), and negative high ("NH") as shown in Figure 4(a). The HESS must meet the positive P_{LF} , which is the power demand, and the negative PLF, which is the excess power that must be taken in by the battery-SC system. Contrarily, the input variable SOC_{sc} only has three MFs, denoted by the letters high (H), medium (M), and low (L) as shown in Figure 4(b). The output variable α , meanwhile, has five

MFs: PH, PL, zero ("Z"), NL, and NH as shown in Figure 4(c). The power ratio that will be delivered to and taken-in by the SC is indicated by the positive and negative membership functions, respectively.

Table 2 includes a list of FLC regulations which is represented in Figure 4. Regardless of the SOCsc situation, when the P_{LF} 's power demand is "L," the power sharing ratio (α) be "Z," as the feable power demand places low strain on the battery. To lower the battery's peak current demand whenever the P_{LF} is positive, α is fixed according to power demand intensity and SOCsc. To restore the SC's charge when the P_{LF} is negative, α is determined with extra power and SOCsc level. To calculate how much electricity the SC and PH will share can be used (15).

$$P_H = \alpha P_{LF} \quad (15)$$

PHF and PH are added to determine the overall power that the SC will supply, or P_{sc}^* .

$$P * SC = P_{HL} + P_H \quad (16)$$

The bidirectional DC-DC converter in the proposed system would control SC power flow in accordance with P_{sc}^* . Therefore, it is anticipated that the battery will deliver the power discrepancy between P_{sc}^* and dP as specified in (17).

$$P_{batt} = dP - P * SC \quad (17)$$

Table 2. Rules of FLC

	dP					
	PH	PL	L	NL	NH	
SOCSC	H	PH	PL	Z	Z	Z
	M	PL	PL	Z	NL	NL
	L	Z	Z	Z	NL	NH

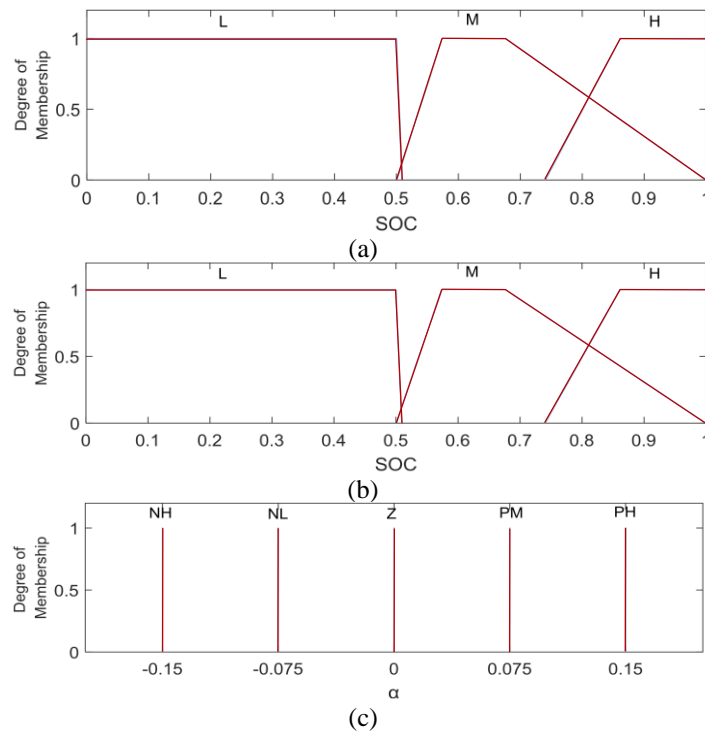


Figure 4. Membership functions: (a) input 1: P_{LF} , (b) input 2: SOCsc, and (c) output: α

3.3.4. Moth flame optimization (MFO) algorithm

The moth-flame optimization approach is based on the transverse orientation mobility of moths in environment. Moth flames can travel great distances in a straight direction at night by regulating a stable angle with regard to the moon, but artificial light may cause the moths to travel in a dangerous spiral path. The moths are candidates for solutions in the MFO algorithm, with the control variable representing their

location in space. Therefore, during each flight, moths function as particles that change their positions and velocities based on their own pbest as well as the collective group's gbest experience (iteration).

The number of variables within every problem decides the size of the particles. A fitness function calculated at the particle's current position determines the quality of the solution for each particle. The FLC may be optimized based on the projected data since the electrical load and RES can both be forecasted. In this investigation, the load demand and RES profile presented in Figures 2(d) and 2(e) are taken as the baseline model. The anticipated RES data and load demand are used to optimize the MFs of the FLC's input variables. Four points together form a complete trapezoidal MF. The first (left) MF and the last (right) MF of a variable with more than two trapezoidal MFs each have just two tuning points. As a result, equation can be used to determine the number of points that are optimal for a given variable n shown as (18).

$$n = (4 \times mf) - 4 \quad (18)$$

mf is the number of MF, in this case. PLF and SOCsc, two input variables, have five and three MFs, respectively, in the suggested control approach. Because of this, the MFO algorithm must optimize 24 points altogether. In light of this, A 24-dimensional particle can be used to represent an FLC or solution. The population size and the number of iterations is user-defined in the MFO procedure, as shown in flowchart.

3.3.5. Fitness function

The battery's high discharge current causes extreme damage since it raises the battery's temperature and the pace at which positive active mass sludges. The major goal is to reduce the battery high current while keeping the SC above 50% of SOCsc. The system's cost can be decreased while also increasing battery efficiency and lifespan due to the reduction in battery peak current [35]–[37]. The fitness function, f , evaluates the solution's fitness in MFO. In this study, the maximum battery current, denoted by $f(x)$, is defined in (19).

$$f(x) = \max(I_{batt}) \quad (19)$$

Where I_{batt} stands for the battery current. The highest battery current of every function is noted for the MFO algorithm to find the best one in each iteration.

4. RESULTS AND DISCUSSION

4.1. MFO algorithm

The fitness value versus iteration count graph is shown in Figure 5. Based on the load profiles depicted in Figure 2, MFO optimizes the MFs of FLC. The flowchart for MFO optimization is shown in Figure 6, where a population size of 20 particles and a total of 80 iterations are specified. Each 24-dimensional particle represents an FLC model. Every particle in the population is regulated using the fitness function, which is described in (19). After each evaluation, the particle's individual best (pbest) and overall best (gbest) are updated.

Using a randomly generated solution, the first iteration's gbest is 6.0282 A. As iterations go longer, the fitness value gets lower. The gbest is maintained at 5.696 A through the 80th iteration after being decreased to that value at the 60th iteration. By the time the optimization procedure is complete, the top choice (the particle with gbest of 5.696 A) has been converted into an FLC model, as shown in Figure 4.

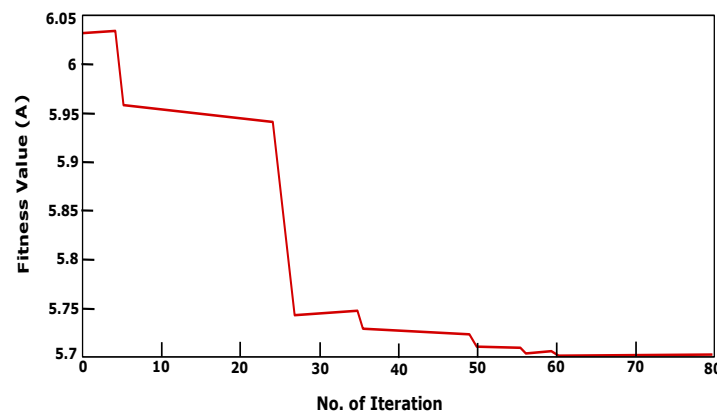


Figure 5. MFO algorithm's convergence curve after 80 iterations of optimization

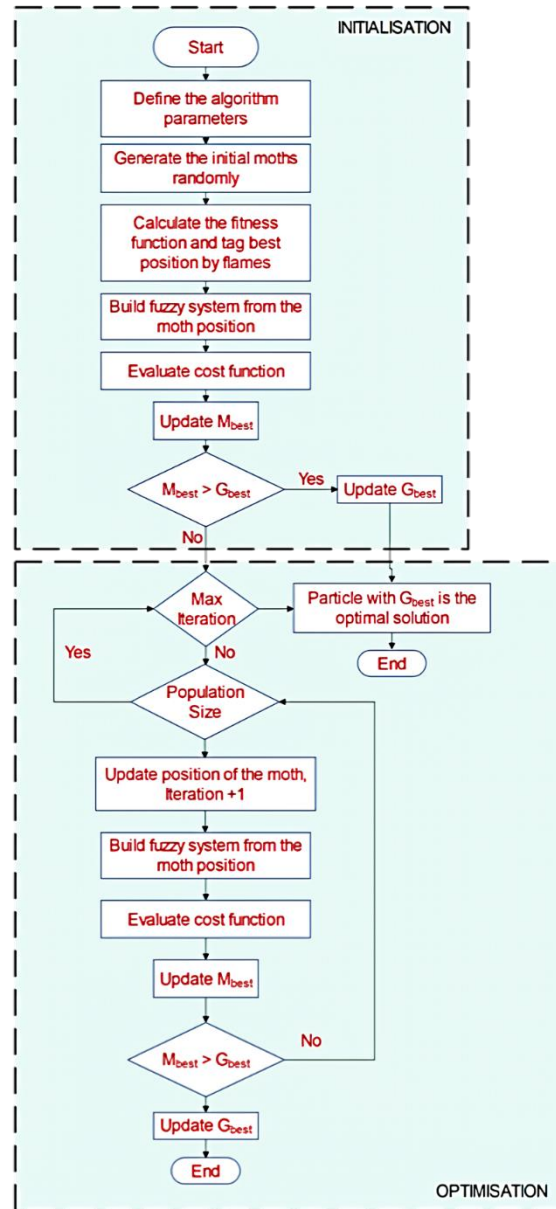


Figure 6. Flowchart of MFO process

4.2. Simulation

Simulink is used in this study to build the three models stated in the Table 3. The solar-wind system with battery-SC model and RBC is referred as model I. The Solar-wind system with battery-SC model and HPF-based FBC is named as model II. The hybrid PV-wind system with battery-SC model and the suggested control approach makes up model III. Table 3 depicts the configuration of the control strategies. The power source and load profiles are modelled and adapted to all models, as shown in Figure 2.

A number of battery metrics are assessed, including average battery SOC ($SOC_{batt \text{ average}}$), peak battery current ($I_{batt \text{ peak}}$), peak battery power ($P_{batt \text{ peak}}$), and final battery SOC ($SOC_{batt \text{ final}}$). Lower battery stress, greater battery efficiency, and a decrease in internal voltage are all effects of reducing $I_{batt \text{ peak}}$ and $P_{batt \text{ peak}}$ [4], [5]. In this study, the $SOC_{batt \text{ average}}$ and $SOC_{batt \text{ final}}$ are examined. Higher $SOC_{batt \text{ average}}$ and $SOC_{batt \text{ final}}$ would increase the life of battery and decrease system LPSP.

$|DP|$ stands for the absolute rate of change of power in a time step of dt , expressed in Watt per second (W/s). To calculate $|DP|$ can be used (20).

$$||\Delta P| = \frac{P(t) - P(t - \Delta t)}{\Delta t}| \quad (20)$$

Where $P(t)$ denotes battery power at time t , $P(t-Dt)$ denotes battery power at time $t-Dt$, and Dt is the study's 1 s time step. In other words, $|DP|$ can be used to estimate the battery power's amount of fluctuation, with a greater value indicating a higher level of variation. Low levels of battery power fluctuation can boost the battery's efficiency and life expectancy. This study computes the battery power's maximum $|DP|$ ($|DP|_{\max}$) and mean $|DP|$ ($|DP|_{\text{mean}}$) to assess the battery's level of dynamic stress.

Table 3. Model configurations

Model	Energy source	Energy storage system	Control strategy
I	PV/Wind	Battery/SC	RBC
II	PV/Wind	Battery/SC	FBC
III	PV/Wind	Battery/SC	FLC/MFO (proposed control strategy)

The simulation model of all battery profiles simulation is shown in Figures 7(a)-(c). Table 4 compares and summarizes each model's battery performance. The $I_{\text{batt peak}}$ and $P_{\text{batt peak}}$ are decreased for Model II, according to Figure 7(b) and Table 4, but the battery still endures a significantly variable power demand. As the SC expends the majority of its energy to deliver the load, the $\text{SOC}_{\text{batt average}}$ and $\text{SOC}_{\text{batt final}}$ are increased by 0.76 percent and 0.01 percent, discretely. These improvements are the largest of all the models. Table 4 and Figure 7(b) for model II demonstrate a notable decrease in the active strain of the battery but only a marginal improvement in $I_{\text{batt peak}}$ and $P_{\text{batt peak}}$. This is due to the FBC, which was created to lessen the dynamic load on the battery without taking peak demand into account. However, the $\text{SOC}_{\text{batt average}}$ and $\text{SOC}_{\text{batt final}}$ are not significantly developed (0%), as the SC only absorbs the highly fluctuating low power components.

As shown in Figure 7, the battery power profile for model III is noticeably smoother than that of Models I and II. SC compensates for the difference between dP and battery power. As previously stated, one of the suggested model's objectives is to attenuate the battery's peak demand. The maximum battery current in Model III in the simulation is 5.696 A, which is identical to the gbest because the MFO optimization and simulation use the same energy source and load profiles.

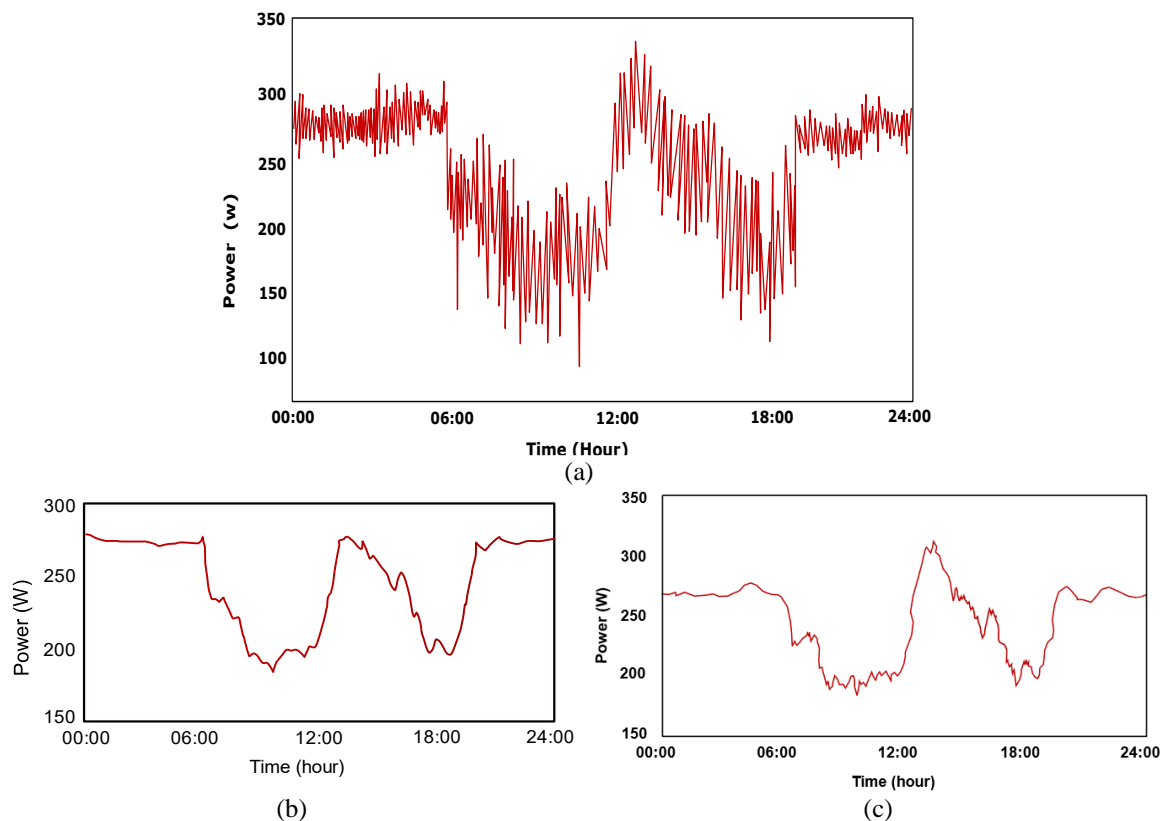


Figure 7. Battery profiles: (a) battery power – model I, (b) battery power – model II, and (c) battery power – model III

Table 4. Summary of battery performance

Battery parameters		Model I	Model II	Model III
I_{batt_peak}	Current (A)	6.053	6.152	5.696
	Attenuation (%)	-	-1.02	5.9
P_{batt_peak}	Power (W)	293.6450	296.5788	275.4768
	Attenuation (%)	-	-1.01	6.19
$SOC_{batt_average}$	SOC (%)	67.3008	66.7895	67.2767
	Increase (%)	-	0.76	0.4
SOC_{batt_final}	SOC (%)	47.8976	47.7657	47.8734
	Increase (%)	-	0.01	1.15
$ \Delta P _{max}$	Rate (ws-1)	24.1243	8.7685	7.4899
	Attenuation (%)	-	74.17	77.01
$ \Delta P _{mean}$	Rate (ws-1)	0.346	0.017869	0.01567
	Attenuation (%)	-	95.01	95.59

Due to the FLC's inclusion in the suggested control plan, the SC delivers to satisfy the high demand while continuously taking its SOC level into account. As a result, when compared to model I, the I_{batt_peak} and P_{batt_peak} are decreased by 5.9 and 6.19 percent, discretely. Since the SC expends the majority of its energy achieving the control strategy's objectives, the $SOC_{batt_average}$ and SOC_{batt_final} are enhanced by 0.4 and 1.15 percent, discretely which is significantly less than model I.

By determining the absolute value of the total ampere-hours (amount of charge) travelling to and from the SC, $|Ah|_{SC}$, it is possible to estimate the SC utilization in the HESS. The SC current is integrated over time to determine the SC ampere-hours. The SOC_{sc} and $|Ah|_{SC}$ of models I, II, and III are shown in Figure 8 during the simulation. The level of battery use decreases as SC utilization increases. As a result, by raising the SC utilization level, the system's internal losses can be decreased as shown in Figure 8(a). By boosting SC use, the system can be made smaller. This is because a significant portion of the resultant current passes via the SC, which has a lower internal resistance and, as a result, causes the battery to heat up less and last longer.

According to Figure 8(b), Model I's final SOC_{sc} is same as the required minimum SOC_{sc} of 50%. On comparison, model I perform the poorest in terms of SC utilization and battery active strain reduction, meaning that it does not properly use the SC. It also consumes the majority of the SC energy. The result is that Model II's total $|Ah|_{SC}$ is 32.65 percent less than Model III but 487.86 percent more than Model I. Only 0.56 percent net SOC_{sc} is used during the simulation, resulting in a final SOC_{sc} of model II of 92.69 percent. In other words, Model II's SC is not fully utilised. In model III, the final SOC_{sc} is kept at a greater level than in model I while being kept 7.45 percent over the required minimum SOC of 50%. In compared to the other models, model III has the greatest total $|Ah|_{SC}$, with model I and model II's respective SC utilization levels being 687.122 percent and 32.65 percent lower. In other words, the suggested technique can run the SC under the specified SOC range and effectively utilize the SC's constricted energy limit to produce promising performance.

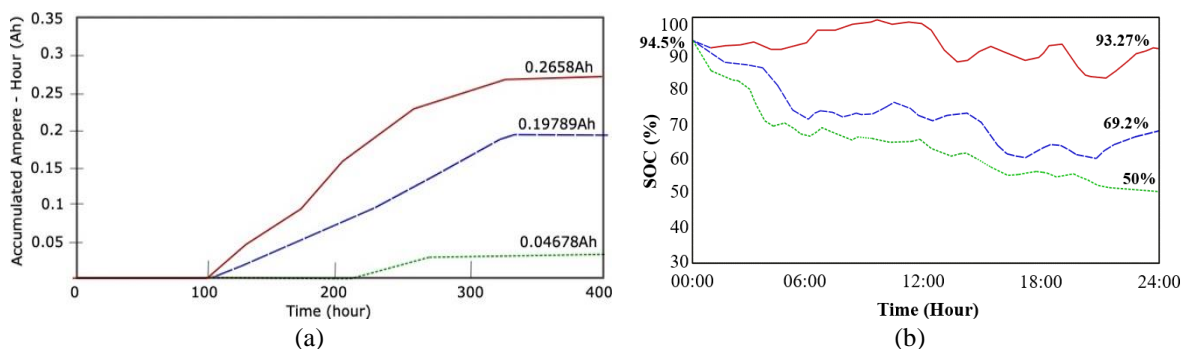


Figure 8. Supercapacitor performance during the course of a 24-hour Simulink simulation (a) accumulated ampere hour of supercapacitor and (b) state of charge of capacitor

The suggested system (model III) is tested using the load profile depicted in Figure 2(b) and various weather conditions. As would be expected, the scenario's most important changes are the decrease in peak demand and strain level of the battery. Regardless of the weather and load profile, the simulation results demonstrate that the suggested method greatly attenuates the battery's active strain ($|\Delta P|_{mean}$) by more than 80% when compared to model I. In the meantime, the decrease in battery's high need depends on the stress

level of dP, which is established by the power source and the load demand. With the high dP and low PV output or peak load demand, the battery peak demand can be significantly reduced as shown in Figure 8 [38].

5. CONCLUSION

An optimal control approach and the Simulink of the proposed solar-wind system with battery-SC model are presented in this study. The system's goals are to decrease the strain and high-power need of the battery by utilizing LPF and FLC. To optimize the reduction of the battery high current, the MFO algorithm is used to adjust the MFs of the FLC. The proposed model is assessed and analyzed with the traditional system using control techniques (RBC and FBC). According to the simulated outcomes, the proposed method significantly reduces the strain and high current need of the battery, by increasing the overall utilization of Supercapacitor which would ultimately increase the battery's lifespan.





REFERENCES

- [1] A. Q. Jakhriani, A. R. H. Rigit, A.-K. Othman, S. R. Samo, and S. A. Kamboh, "Life cycle cost analysis of a standalone PV system," in *2012 International Conference on Green and Ubiquitous Technology*, Jul. 2012, pp. 82–85. doi: 10.1109/GUT.2012.6344195.
- [2] S. Y. Kan, M. Verwaal, and H. Broekhuizen, "The use of battery–capacitor combinations in photovoltaic powered products," *Journal of Power Sources*, vol. 162, no. 2, pp. 971–974, Nov. 2006, doi: 10.1016/j.jpowsour.2005.07.001.
- [3] J. Schiffer, D. U. Sauer, H. Bindner, T. Cronin, P. Lundsager, and R. Kaiser, "Model prediction for ranking lead-acid batteries according to expected lifetime in renewable energy systems and autonomous power-supply systems," *Journal of Power Sources*, vol. 168, no. 1, pp. 66–78, May 2007, doi: 10.1016/j.jpowsour.2006.11.092.
- [4] A. C. Baisden and A. Emadi, "Advisor-based model of a battery and an ultra-capacitor energy source for hybrid electric vehicles," *IEEE Transactions on Vehicular Technology*, vol. 53, no. 1, pp. 199–205, Jan. 2004, doi: 10.1109/TVT.2003.822004.
- [5] R. A. Dougal, S. Liu, and R. E. White, "Power and life extension of battery-ultracapacitor hybrids," *IEEE Transactions on Components and Packaging Technologies*, vol. 25, no. 1, pp. 120–131, Mar. 2002, doi: 10.1109/6144.991184.
- [6] S. Pay and Y. Baghzouz, "Effectiveness of battery-supercapacitor combination in electric vehicles," in *2003 IEEE Bologna Power Tech Conference Proceedings*, 2003, vol. 3, pp. 728–733. doi: 10.1109/PTC.2003.1304472.
- [7] Z. Song, H. Hofmann, J. Li, J. Hou, X. Han, and M. Ouyang, "Energy management strategies comparison for electric vehicles with hybrid energy storage system," *Applied Energy*, vol. 134, pp. 321–331, Dec. 2014, doi: 10.1016/j.apenergy.2014.08.035.
- [8] N. Altin and İ. Sefa, "dSPACE based adaptive neuro-fuzzy controller of grid interactive inverter," *Energy Conversion and Management*, vol. 56, pp. 130–139, Apr. 2012, doi: 10.1016/j.enconman.2011.11.017.
- [9] A. T. Azar, *Fuzzy systems*. InTech, 2010. doi: 10.5772/133.
- [10] A. Mellit and A. M. Pavan, "A 24-h forecast of solar irradiance using artificial neural network: Application for performance prediction of a grid-connected PV plant at Trieste, Italy," *Solar Energy*, vol. 84, no. 5, pp. 807–821, May 2010, doi: 10.1016/j.solener.2010.02.006.
- [11] Y. El Mghouchi, T. Ajzoul, and A. El Bouardi, "Prediction of daily solar radiation intensity by day of the year in twenty-four cities of Morocco," *Renewable and Sustainable Energy Reviews*, vol. 53, pp. 823–831, Jan. 2016, doi: 10.1016/j.rser.2015.09.059.
- [12] Y. El Mghouchi, T. Ajzoul, D. Taoukil, and A. El Bouardi, "The most suitable prediction model of the solar intensity, on horizontal plane, at various weather conditions in a specified location in Morocco," *Renewable and Sustainable Energy Reviews*, vol. 54, pp. 84–98, Feb. 2016, doi: 10.1016/j.rser.2015.09.089.
- [13] K. Y. Lee, Y. T. Cha, and J. H. Park, "Short-term load forecasting using an artificial neural network," *IEEE Transactions on Power Systems*, vol. 7, no. 1, pp. 124–132, 1992, doi: 10.1109/59.141695.
- [14] M. Kumar, "Short-term load forecasting using artificial neural network techniques," 2009. [Online]. Available: http://thesis.nitrkl.ac.in/1303/1/btech_project_final_STLF_using_ANN.pdf
- [15] D. C. Park, M. A. El-Sharkawi, R. J. Marks, L. E. Atlas, and M. J. Damborg, "Electric load forecasting using an artificial neural network," *IEEE Transactions on Power Systems*, vol. 6, no. 2, pp. 442–449, May 1991, doi: 10.1109/59.76685.
- [16] The MathWorks, "Mamdani and sugeno fuzzy inference systems," 2016. <https://www.mathworks.com/help/fuzzy/types-of-fuzzy-inference-systems.html>
- [17] Y. D. Song, Q. Cao, X. Du, and H. R. Karimi, "Control strategy based on wavelet transform and neural network for hybrid power system," *Journal of Applied Mathematics*, vol. 2013, pp. 1–8, 2013, doi: 10.1155/2013/375840.
- [18] R. Pecan and A. Nayir, "Design and implementation of a 12-kW wind-solar distributed power and instrumentation system as an educational testbed for electrical engineering technology students," in *2010 Modern Electric Power Systems*, Wroclaw, 2010, pp. 1–6. [Online]. Available: <https://ieeexplore.ieee.org/document/6007240>
- [19] R. Lu, C. Zhu, L. Tian, and Q. Wang, "Super-capacitor stacks management system with dynamic equalization techniques," *IEEE Transactions on Magnetics*, vol. 43, no. 1, pp. 254–258, 2007, doi: 10.1109/TMAG.2006.887652.
- [20] P. García, C. A. García, L. M. Fernández, F. Llorens, and F. Jurado, "ANFIS-based control of a grid-connected hybrid system integrating renewable energies, hydrogen and batteries," *IEEE Transactions on Industrial Informatics*, vol. 10, no. 2, pp. 1107–1117, 2014, doi: 10.1109/TII.2013.2290069.
- [21] P. García, J. P. Torreglosa, L. M. Fernández, and F. Jurado, "Optimal energy management system for stand-alone wind turbine/photovoltaic/hydrogen/battery hybrid system with supervisory control based on fuzzy logic," *International Journal of Hydrogen Energy*, vol. 38, no. 33, pp. 14146–14158, Nov. 2013, doi: 10.1016/j.ijhydene.2013.08.106.
- [22] S. Wang et al., "Design and advanced control strategies of a hybrid energy storage system for the grid integration of wind power generations," *IET Renewable Power Generation*, vol. 9, no. 2, pp. 89–98, Mar. 2015, doi: 10.1049/iet-rpg.2013.0340.
- [23] M. Sarvi and I. N. Avanaki, "An optimized fuzzy logic controller by water cycle algorithm for power management of stand-alone hybrid green power generation," *Energy Conversion and Management*, vol. 106, pp. 118–126, Dec. 2015, doi: 10.1016/j.enconman.2015.09.021.





- [24] R. Yumurtaci, "Role of energy management in hybrid renewable energy systems: case study based analysis considering varying seasonal conditions," *TURKISH JOURNAL OF ELECTRICAL ENGINEERING & COMPUTER SCIENCES*, vol. 21, no. 4, pp. 1077–1091, 2013, doi: 10.3906/elk-1112-85.
- [25] M. H. Athari and M. M. Ardehali, "Operational performance of energy storage as function of electricity prices for on-grid hybrid renewable energy system by optimized fuzzy logic controller," *Renewable Energy*, vol. 85, pp. 890–902, Jan. 2016, doi: 10.1016/j.renene.2015.07.055.
- [26] S. Safari, M. M. Ardehali, and M. J. Sirizi, "Particle swarm optimization based fuzzy logic controller for autonomous green power energy system with hydrogen storage," *Energy Conversion and Management*, vol. 65, pp. 41–49, Jan. 2013, doi: 10.1016/j.enconman.2012.08.012.
- [27] R. Cozzolino, L. Tribioli, and G. Bella, "Power management of a hybrid renewable system for artificial islands: A case study," *Energy*, vol. 106, pp. 774–789, Jul. 2016, doi: 10.1016/j.energy.2015.12.118.
- [28] V. Dash and P. Bajpai, "Power management control strategy for a stand-alone solar photovoltaic-fuel cell-battery hybrid system," *Sustainable Energy Technologies and Assessments*, vol. 9, pp. 68–80, Mar. 2015, doi: 10.1016/j.seta.2014.10.001.
- [29] A. Brka, G. Kothapalli, and Y. M. Al-Abdeli, "Predictive power management strategies for stand-alone hydrogen systems: Lab-scale validation," *International Journal of Hydrogen Energy*, vol. 40, no. 32, pp. 9907–9916, Aug. 2015, doi: 10.1016/j.ijhydene.2015.06.081.
- [30] M. A. Akcayol, "Application of adaptive neuro-fuzzy controller for SRM," *Advances in Engineering Software*, vol. 35, no. 3–4, pp. 129–137, Mar. 2004, doi: 10.1016/j.advengsoft.2004.03.005.
- [31] F. Garcia-Torres and C. Bordons, "Optimal economical schedule of hydrogen-based microgrids with hybrid storage using model predictive control," *IEEE Transactions on Industrial Electronics*, vol. 62, no. 8, pp. 5195–5207, Aug. 2015, doi: 10.1109/TIE.2015.2412524.
- [32] A. Kuperman and I. Aharon, "Battery-ultracapacitor hybrids for pulsed current loads: A review," *Renewable and Sustainable Energy Reviews*, vol. 15, no. 2, pp. 981–992, Feb. 2011, doi: 10.1016/j.rser.2010.11.010.
- [33] Y. Zhang, Z. Jiang, and X. Yu, "Control strategies for battery/supercapacitor hybrid energy storage systems," in *2008 IEEE Energy 2030 Conference*, Nov. 2008, pp. 1–6. doi: 10.1109/ENERGY.2008.4781031.
- [34] N. Mendis, K. M. Muttaqi, and S. Perera, "Active power management of a super capacitor-battery hybrid energy storage system for standalone operation of DFIG based wind turbines," in *2012 IEEE Industry Applications Society Annual Meeting*, Oct. 2012, pp. 1–8. doi: 10.1109/IAS.2012.6374045.
- [35] N. Omar, J. Van Mierlo, B. Verbrugge, and P. Van den Bossche, "Power and life enhancement of battery-electrical double layer capacitor for hybrid electric and charge-depleting plug-in vehicle applications," *Electrochimica Acta*, vol. 55, no. 25, pp. 7524–7531, Oct. 2010, doi: 10.1016/j.electacta.2010.03.039.
- [36] P. Lailler *et al.*, "Study of the softening of the positive active-mass in valve-regulated lead-acid batteries for electric-vehicle applications," *Journal of Power Sources*, vol. 78, no. 1–2, pp. 204–213, Mar. 1999, doi: 10.1016/S0378-7753(99)00038-5.
- [37] P. Ruetschi, "Aging mechanisms and service life of lead-acid batteries," *Journal of Power Sources*, vol. 127, no. 1–2, pp. 33–44, Mar. 2004, doi: 10.1016/j.jpowsour.2003.09.052.
- [38] G. Papazov and D. Pavlov, "Influence of cycling current and power profiles on the cycle life of lead/acid batteries," *Journal of Power Sources*, vol. 62, no. 2, pp. 193–199, Oct. 1996, doi: 10.1016/S0378-7753(96)02422-6.

BIOGRAPHIES OF AUTHORS



V. Prasanna     is currently a research scholar in Department of Electrical and Electronics Engineering, Puducherry Technological University (PTU), Puducherry, India. He has done B.E. in Electrical Engineering from Panimalar Engineering College, Chennai, and his M.Tech. from Pondicherry Engineering College (PEC), Puducherry. His main research directions include hybrid energy storage system (HESS), power quality in power systems (PEPS). He can be contacted at email: prasannav@ptuniv.edu.in.



G. Ravi     received his B.E. degree in Electrical and Electronics Engineering from Mysore University in 1992, his M.E. degree from Annamalai University in 1994, and Ph.D. degree from Jadavpur University in 2005. At present he is Professor in Electrical and Electronics Engineering Department at Puducherry Technological University, Pondicherry India. His research area includes artificial intelligent techniques, electrical machines, power system operation, planning and optimization, and power quality. He can be contacted at email: ravig@ptuniv.edu.in.